

Total Variation-Penalized Poisson Likelihood Estimation for Ill-Posed Problems

Johnathan M. Bardsley^{† ‡}

Department of Mathematical Sciences, University of Montana, Missoula, MT.

Email: bardsleyj@mso.umt.edu

Aaron Luttmann

Division of Science and Mathematics, Bethany Lutheran College, Mankato, MN.

Email: luttmann@blc.edu

Abstract. The noise contained in data measured by imaging instruments is often primarily of Poisson type. This motivates, in many cases, the use of the Poisson negative-log likelihood function in place of the ubiquitous least squares data fidelity when solving image deblurring problems. We assume that the underlying blurring operator is compact, so that, as in the least squares case, the resulting minimization problem is ill-posed and must be regularized. In this paper, we focus on total variation regularization and show that the problem of computing the minimizer of the resulting total variation-penalized Poisson likelihood functional is well-posed. We then prove that, as the errors in the data and in the blurring operator tend to zero, the resulting minimizers converge to the minimizer of the exact likelihood function. Finally, the practical effectiveness of the approach is demonstrated on synthetically generated data, and a nonnegatively constrained, projected quasi-Newton method is introduced.

PACS numbers: 02.30.Zz, 02.50.-r, 07.05.Pj

Keywords: total variation regularization, ill-posed problems, maximum likelihood estimation, image deblurring, nonnegatively constrained minimization.

1. Introduction

We consider the problem of solving

$$z = Au \stackrel{\text{def}}{=} \int_{\Omega} a(x, y; \xi, \eta) u(\xi, \eta) d\xi d\eta, \quad (1)$$

for u on a bounded domain Ω . We assume $a \in L^2(\Omega)$ so that $A : L^p(\Omega) \rightarrow L^2(\Omega)$ is a compact linear operator for all $p \geq 1$. We also assume that the exact data z is nonnegative and in $L^\infty(\Omega)$, in which case solving (1) is an ill-posed problem [20, 22]. Finally, we denote the true solution by u_{exact} and assume that it is a solution of (1).

[†] To whom correspondence should be addressed.

[‡] This work was supported by the NSF under grant DMS-0504325.

1.1. Discretization Error

In practical applications, e.g. astronomy and medical imaging, the continuous image z in (1) is sampled via a charge coupled device (CCD) camera on a uniform grid. Without loss of generality, we assume that this grid is defined by the $N \times N$ array of points

$$\{(x_i, y_j) \mid x_i = (2i - 1)/2N, \quad y_j = (2j - 1)/2N, \quad 1 \leq i, j \leq N\},$$

which are the centers of the pixels

$$\Omega_{ij} = \{(x, y) \mid (i - 1)/N \leq x \leq i/N, \quad (j - 1)/N \leq y \leq j/N\}, \quad 1 \leq i, j \leq N,$$

of the CCD array. The CCD camera estimates the value of z within Ω_{ij} by counting the number of photons emitted from the object incident upon Ω_{ij} . If the number of photons is counted exactly, this will yield the total intensity of the image within Ω_{ij} , which is given, using (1) and Fubini's theorem, by

$$\int_{\Omega_{ij}} z(x, y) dx dy = \int_{\Omega} \left(\int_{\Omega_{ij}} a(x, y; \xi, \eta) dx dy \right) u(\xi, \eta) d\xi d\eta. \quad (2)$$

Using midpoint quadrature in the x, y variables on both the left and right-hand sides of (2) and ignoring quadrature error yields

$$z(x_i, y_j) = \int_{\Omega} a(x_i, y_j; \xi, \eta) u(\xi, \eta) d\xi d\eta.$$

Applying midpoint quadrature once again in the ξ, η variables yields, finally, the system of equations

$$z(x_i, y_j) = \frac{1}{N^2} \sum_{r=1}^N \sum_{s=1}^N a(x_i, y_j; \xi_r, \eta_s) u(\xi_r, \eta_s) + \epsilon_{ij}^{\text{quad}}, \quad 1 \leq i, j \leq N, \quad (3)$$

where $\epsilon_{ij}^{\text{quad}}$ is quadrature error at the ij th grid point. Note that we have assumed co-location of grid points in the x, y and ξ, η planes.

In practical applications, estimates of the array values $\{u(\xi_r, \eta_s)\}_{r,s=1}^N$ are sought from noisy measurements $\{z_{ij}\}_{i,j=1}^N$ of $\{z(x_i, y_j)\}_{i,j=1}^N$. Defining $a_{ij}(\xi, \eta) := a(x_i, y_j; \xi_r, \eta_s)$, we can then write (3) as

$$z_{ij} = \frac{1}{N^2} \sum_{r=1}^N \sum_{s=1}^N a_{ij}(\xi_r, \eta_s) u(\xi_r, \eta_s) + \epsilon_{ij}^{\text{quad}} + \epsilon_{ij}^{\text{stoch}}, \quad 1 \leq i, j \leq N, \quad (4)$$

where $\epsilon_{ij}^{\text{stoch}}$ is the stochastic error at the ij th grid point that arises due to the measurement noise. In this paper, we present and analyze an approach for estimating $\{u(\xi_r, \eta_s)\}_{r,s=1}^N$ that incorporates a noise model for $\epsilon_{ij}^{\text{stoch}}$.

1.2. Poisson Likelihood Estimation

In order to better model the errors contained in the data measurements $\{z_{ij}\}_{i,j=1}^N$, we use the statistical model for CCD camera measurement error given in [18, 19]:

$$z_{ij} \sim \text{Poiss} \left(\int_{\Omega_{ij}} z(x, y) dx dy \right) + \text{Poiss}(\gamma) + N(0, \sigma^2). \quad (5)$$

By (5), we mean that

$$z_{ij} \sim n_{\text{obj}}(i, j) + n_0(i, j) + g(i, j), \quad i = 1, \dots, N^2, \quad (6)$$

where

- $n_{\text{obj}}(i, j)$ is the number of object dependent photoelectrons measured by the ij th detector in the CCD array. It is a Poisson random variable with Poisson parameter $\int_{\Omega_{ij}} z(x, y) dx dy$.
- $n_0(i, j)$ is the number of background photoelectrons, which arise from both natural and artificial sources, measured by the ij th detector in the CCD array. It is a Poisson random variable with a fixed positive Poisson parameter γ .
- $g(i, j)$ is the so-called readout noise, which is due to random errors caused by the CCD electronics and errors in the analog-to-digital conversion of measured voltages. It is a Gaussian random variable with mean 0 and fixed variance σ^2 .

The random variables $n_{\text{obj}}(i, j)$, $n_0(i, j)$, and $g(i, j)$ are assumed to be independent of one another and of $n_{\text{obj}}(r, s)$, $n_0(r, s)$, and $g(r, s)$ for $r \neq i$ or $s \neq j$.

Now, if we ignore quadrature error in (4), and assume that our error model is given by (5), we obtain the statistical model

$$z_{ij} \sim \text{Poiss} \left(\frac{1}{N^2} \sum_{r=1}^N \sum_{s=1}^N a_{ij}(\xi_r, \eta_s) u(\xi_r, \eta_s) \right) + \text{Poiss}(\gamma) + N(0, \sigma^2), \quad (7)$$

for data collection. As in [18], we use the approximation

$$N(\sigma^2, \sigma^2) \approx \text{Poiss}(\sigma^2), \quad (8)$$

to obtain, from (7),

$$z_{ij} + \sigma^2 \sim \text{Poiss} \left(\left(\frac{1}{N^2} \sum_{r=1}^N \sum_{s=1}^N a_{ij}(\xi_r, \eta_s) u(\xi_r, \eta_s) \right) + \gamma + \sigma^2 \right), \quad (9)$$

The maximum likelihood estimate of u_{exact} on the computational grid is then given by minimizing

$$\sum_{i=1}^N \sum_{j=1}^N \left\{ \left[\left(\frac{1}{N^2} \sum_{r=1}^N \sum_{s=1}^N a_{ij}(\xi_r, \eta_s) u(\xi_r, \eta_s) \right) + \gamma + \sigma^2 \right] - (z_{ij} + \sigma^2) \log \left[\left(\frac{1}{N^2} \sum_{r=1}^N \sum_{s=1}^N a_{ij}(\xi_r, \eta_s) u(\xi_r, \eta_s) \right) + \gamma + \sigma^2 \right] \right\} \quad (10)$$

with respect to the array $\{u(\xi_r, \eta_s)\}_{r,s=1}^N$. Before continuing, we note that in practice, using the negative-log of the Poisson likelihood (10) instead of the least squares likelihood can yield much improved results, particularly if the object is composed of sub-objects with a wide range of intensities (see e.g., the results in [5]).

Our solution method proposes the use of (10) as the data-fidelity function. In order to handle the difficulties that arise due to the ill-posedness of problem (1), we will use total variation regularization. The resulting computational problem is of interest, and

we will devote a significant portion our work to the development of an efficient method for this problem. It is also essential, however, that we perform a rigorous theoretical analysis (i.e. in a function space setting) of the method. Such a theoretical analysis is important because it will allow us to trust the results obtained in practice. Furthermore, in the functional analytic setting, the effect of the regularization functional is easier to quantify; in particular, the regularization functional determines the function space within which the regularized solutions will lie.

1.3. The Functional Analogue of the Poisson Negative-Log Likelihood

The functional analogue of (10) can be obtained by removing both stochastic and quadrature errors from the discrete model. In theory, stochastic errors can be removed by computing the mean of samples from (5) as the sample size tends to infinity. The result, by the Central Limit Theorem, is

$$\int_{\Omega_{ij}} z(x, y) dx dy + \gamma.$$

Quadrature errors, on the other hand, are removed by letting the number of grid points tend to infinity. A simultaneous removal of these two types of error yield, via standard integral convergence arguments, the convergence of (10) to

$$T_0(Au; z + \gamma) = \int_{\Omega} ((Au + \gamma + \sigma^2) - (z + \gamma + \sigma^2) \log(Au + \gamma + \sigma^2)) dx dy, \quad (11)$$

where z and A are as defined in equation (1); that is, they are the exact data function and integral operator respectively.

Before continuing, we emphasize that z is defined over all of Ω , while z_{ij} is a noisy measurements of the total intensity of z over Ω_{ij} .

The unique minimizer of T_0 is u_{exact} . To see this, we compute the gradient and Hessian of T_0 with respect to u , which are given, respectively, by

$$\nabla T_0(Au; z + \gamma) = A^* \left(\frac{Au - z}{Au + \gamma + \sigma^2} \right), \quad (12)$$

$$\nabla^2 T_0(Au; z + \gamma) = A^* \left(\text{diag} \left(\frac{z + \gamma + \sigma^2}{(Au + \gamma + \sigma^2)^2} \right) \right) A, \quad (13)$$

where “ $*$ ” denotes operator adjoint, and $\text{diag}(v)$ is the linear operator defined by $\text{diag}(v)w \stackrel{\text{def}}{=} vw$. Since $z \geq 0$ (see comments following (1)), $\nabla^2 T_0$ is a positive definite operator. Thus T_0 is strictly convex [22, Theorem 2.42], with unique minimizer u_{exact} as desired.

1.4. Total Variation Regularization

Due to the fact that A is compact, the problem of computing the minimizer of T_0 is an ill-posed problem and must be regularized [22, 20]. This involves replacing $T_0(Au; z + \gamma)$ by the parameter dependent functional

$$T_{\alpha}(Au; z + \gamma) \stackrel{\text{def}}{=} T_0(Au; z + \gamma) + \alpha J(u), \quad (14)$$

where $\alpha > 0$ is the regularization parameter and J the regularization functional, which provides stability and incorporates prior knowledge about the exact solution. If the exact solution is known to have jump discontinuities, as we will assume in this paper, one can use total variation regularization [1, 23]. In theory, this is accomplished by taking

$$J(u) = J_\beta(u) \stackrel{\text{def}}{=} \sup_{v \in \mathcal{V}} \int_{\Omega} \left(-u \nabla \cdot v + \sqrt{\beta(1 - |v(x)|^2)} \right) dx, \quad (15)$$

where $\beta \geq 0$ and

$$\mathcal{V} = \{v \in C_0^1(\Omega; \mathbb{R}^d) : |v(x)| \leq 1 \quad x \in \Omega\}.$$

We note that if u is continuously differentiable on Ω , (15) takes the recognizable form [1, Theorem 2.1]

$$J_\beta(u) \stackrel{\text{def}}{=} \int_{\Omega} \sqrt{|\nabla u|^2 + \beta} dx. \quad (16)$$

$J_0(u)$ is known as the *total variation* of u .

When (15) is used, minimizers of T_α will lie (as we will show later) in the space of functions of bounded variation on Ω , which is defined by

$$BV(\Omega) = \{u \in L^1(\Omega) : J_0(u) < \infty\}. \quad (17)$$

We will assume that $u_{\text{exact}} \in BV(\Omega)$. Furthermore, since $u_{\text{exact}} \geq 0$, a nonnegativity constraint is natural. This gives, finally, the exact regularized minimization problem

$$\arg \min_{u \in \mathcal{C}} T_\alpha(Au; z + \gamma), \quad (18)$$

where

$$\mathcal{C} = \{u \in BV(\Omega) \mid u \geq 0 \text{ almost everywhere}\}. \quad (19)$$

At first, the appearance of the exact data z and operator A in (18) may seem confusing. However, our analysis will show that solutions of (18), (19) are stable with respect to small perturbations in z and A . With this result in hand, we can conclude that even if noisy measurements of both z and a are used in practice, one can expect our method to yield a regularized solution that well-approximates u_{exact} given the noise level and an appropriately chosen regularization parameter.

1.5. Paper Objectives

We will present our theoretical analysis in Section 2. In particular, we will provide justification for using (18), (19). This will involve first proving that (18), (19) is a well-posed problem, i.e. that (18) has a unique solution $u_\alpha \in \mathcal{C}$ for each $\alpha > 0$, and that given a sequence of perturbed problems

$$z_n(x, y) = A_n u(x, y) \stackrel{\text{def}}{=} \int_{\Omega} a_n(x, y; \xi, \eta) u(\xi, \eta) d\xi d\eta, \quad (20)$$

with solutions $u_{\alpha, n}$ of the corresponding minimization problems

$$\arg \min_{u \in \mathcal{C}} T_\alpha(A_n u; z_n), \quad (21)$$

$u_{\alpha,n} \rightarrow u_\alpha$ provided $A_n \rightarrow A$ and $z_n \rightarrow z + \gamma$. We also must show that a sequence of positive regularization parameters $\{\alpha_n\}$ can be chosen so that $u_{\alpha_n,n} \rightarrow u_{\text{exact}}$ as $\alpha_n \rightarrow 0$, where $u_{\alpha_n,n}$ is the minimizer of T_{α_n} over \mathcal{C} .

In Section 3, we focus on the computational problem that must be solved when the above method is used in practice. The problem is non-trivial due to the presence of the nonnegativity constraint and the total-variation regularization, so a highly robust method is required. To this end, we present a nonnegatively constrained, projected quasi-Newton minimization algorithm. The method is similar to the projected Newton method [7], but with the projected Hessian replaced by a projected quasi-Newton approximation motivated by the approximation used in the quasi-Newton formulation of the lagged-diffusivity fixed point iteration [23].

We end the paper with conclusions in Section 4.

2. Theoretical Analysis

We begin with definitions and results that will be needed in our later analysis.

Let Ω and \mathcal{C} be as defined in the introduction. Then $|\Omega| = \int_\Omega dx < \infty$. We will assume that $u_{\text{exact}} \in \mathcal{C}$ and that $Au \geq 0$ for every $u \in \mathcal{C}$, so $z = Au_{\text{exact}} \geq 0$. We make the further assumption that $z \in L^\infty(\Omega)$. Note that these are reasonable assumptions on A and z for imaging applications.

Let $|\cdot|$ denote the Euclidean norm in \mathbb{R}^d and $\|\cdot\|_p$ the Banach space norm on $L^p(\Omega)$ for $1 \leq p \leq \infty$. Since Ω is bounded, $L^p(\Omega) \subset L^1(\Omega)$, $p > 1$.

We now give a number of results and definitions regarding $BV(\Omega)$. First of all, $BV(\Omega)$ is a Banach space with respect to the norm

$$\|u\|_{BV} = \|u\|_1 + J_0(u).$$

Since $\sqrt{x} \leq \sqrt{x+\beta} \leq \sqrt{x} + \sqrt{\beta}$ for $\beta, x \geq 0$, we have

$$J_0(u) \leq J_\beta(u) \leq J_0(u) + \sqrt{\beta}|\Omega|. \quad (22)$$

Inequality (22) will allow us to assume, without loss of generality, that $\beta = 0$ in several of our arguments.

A set $\mathcal{S} \subset BV(\Omega)$ is said to be *BV-bounded* if there exists $M > 0$ such that $\|u\|_{BV} \leq M$ for all $u \in \mathcal{S}$.

A functional $T : L^p(\Omega) \rightarrow \mathbb{R}$ is said to be *BV-coercive* if

$$T(u) \rightarrow +\infty \quad \text{whenever} \quad \|u\|_{BV} \rightarrow +\infty. \quad (23)$$

Note that $BV(\Omega) \subset L^1(\Omega)$, by definition. Also, as a consequence of the following theorem, whose proof is found in [1], $BV(\Omega) \subset L^p(\Omega)$ for $1 \leq p \leq d/(d-1)$, where $d/(d-1) \stackrel{\text{def}}{=} +\infty$ for $d = 1$.

Theorem 1. *Let \mathcal{S} be a BV-bounded set of functions. Then \mathcal{S} is relatively compact, i.e. its closure is compact, in $L^p(\Omega)$ for $1 \leq p < d/(d-1)$. \mathcal{S} is bounded and thus relatively weakly compact for dimensions $d \geq 2$ in $L^p(\Omega)$ for $p = d/(d-1)$.*

2.1. Well-Posedness

We now prove that problem (18), (19) is well-posed for $\alpha > 0$. In order to simplify the notation in our arguments, we will use $T_\alpha(u)$ to denote $T_\alpha(Au; z + \gamma)$ and $T_{\alpha,n}(u)$ to denote $T_\alpha(A_n u; z_n)$ throughout the remainder of the paper.

2.1.1. Existence and Uniqueness of Solutions. In order to prove the existence and uniqueness of solutions of (18), (19), we will use the following theorem, which is similar to [1, Theorem 3.1].

Theorem 2. *If $T : L^p(\Omega) \rightarrow \mathbb{R}$ is strictly convex and BV -coercive, and $1 \leq p \leq d/(d-1)$, then T has a unique minimizer on \mathcal{C} .*

Proof. Let $\{u_n\} \subset \mathcal{C}$ be such that $T(u_n) \rightarrow \inf_{u \in \mathcal{C}} T(u)$. Then $T(u_n)$ is bounded, and hence, by (23), $\{u_n\}$ is BV -bounded. Theorem 1 implies that there exists a subsequence $\{u_{n_j}\}$ that converges to some $\hat{u} \in L^p(\Omega)$. Convergence is weak if $p = d/(d-1)$. Since T is strictly convex, it is weakly lower semi-continuous [24], and hence,

$$T(\hat{u}) \leq \liminf T(u_{n_j}) = \lim T(u_n) = T_*,$$

where T_* is the infimum of T on \mathcal{C} . Thus \hat{u} minimizes T on \mathcal{C} and is unique since T is a strictly convex functional and \mathcal{C} is a convex set. \square

In order to use Theorem 2, we must show that T_α (as defined in (14)) is both strictly convex and BV -coercive.

Lemma 1. *T_α is strictly convex.*

Proof. In the introduction it was shown that T_0 is strictly convex. The strict convexity of T_α then follows immediately from the fact that J_β is convex, which is proved in [1]. \square

Lemma 2. *T_α is BV -coercive on \mathcal{C} .*

Proof. By (23), we must show that if $\|u\|_{BV} \rightarrow \infty$, then $T_\alpha(u) \rightarrow \infty$. A straightforward computation yields the following decomposition of a function $u \in BV(\Omega)$:

$$u = v + w, \tag{24}$$

where

$$w = \left(\int_\Omega u \, dx / |\Omega| \right) \chi_\Omega, \quad \text{and} \quad \int_\Omega v \, dx = 0. \tag{25}$$

Here χ_Ω is the indicator function on Ω . It is shown in [1] that there exists $C_1 \in \mathbb{R}^+$ such that

$$\|v\|_p \leq C_1 J_0(v), \tag{26}$$

for $1 \leq p \leq d/(d-1)$. Equation (26), the triangle inequality, and the fact that $J_0(w) = 0$ yield

$$\|u\|_{BV} \leq \|w\|_1 + (C_1 + 1)J_0(v). \tag{27}$$

Thus if $\|u\|_{BV} \rightarrow \infty$, either $\|w\|_1 \rightarrow \infty$ or $J_0(v) \rightarrow \infty$.

Since $T_\alpha(u) \geq T_0(u_{\text{exact}}) + \alpha J_0(v)$, we see that $J_0(v) \rightarrow \infty$ implies $T_\alpha(u) \rightarrow \infty$. If $\|u\|_{BV} \rightarrow \infty$ and $J_0(v)$ is bounded, from (27) we have $\|w\|_1 \rightarrow \infty$. Noting that

$$\|Aw\|_1 = (\|A\chi_\Omega\|_1 / |\Omega|) \|w\|_1 = C_2 \|w\|_1, \quad (28)$$

since $Au \geq 0$ for all $u \in \mathcal{C}$, Jensen's inequality together with (26) and (28) yields

$$\begin{aligned} T_\alpha(u) &\geq \|Au + \gamma + \sigma^2\|_1 - \|z + \gamma + \sigma^2\|_\infty \log \|Au + \gamma + \sigma^2\|_1, \quad (29) \\ &\geq \|Aw\|_1 - \|Av\|_1 - (\gamma + \sigma^2)|\Omega| \\ &\quad - \|z + \gamma + \sigma^2\|_\infty \log (\|Aw\|_1 + \|Av\|_1 + (\gamma + \sigma^2)|\Omega|), \\ &\geq C_2 \|w\|_1 - \|A\|_1 C_1 J_0(v) - (\gamma + \sigma^2)|\Omega| \\ &\quad - \|z + \gamma + \sigma^2\|_\infty \log (C_2 \|w\|_1 + \|A\|_1 C_1 J_0(v) + (\gamma + \sigma^2)|\Omega|), \\ &\geq C_2 \|w\|_1 - M - \|z + \gamma + \sigma^2\|_\infty \log (C_2 \|w\|_1 + M), \quad (30) \end{aligned}$$

where M is an upper bound of $\|A\|_1 C_1 J_0(v) + (\gamma + \sigma^2)|\Omega|$, and $\|A\|_1$ is the operator norm induced by the norm on $L^1(\Omega)$. From (30), we see that $T_\alpha(u) \rightarrow \infty$ if $\|w\|_1 \rightarrow \infty$, which completes the proof. \square

Existence and uniqueness of solutions of (18), (19) now follows immediately.

Theorem 3 (Existence and Uniqueness of Minimizers). *T_α has a unique minimizer over \mathcal{C} .*

Before continuing, we note that in the denoising case, i.e. when A is the identity operator, the existence and uniqueness of minimizers of $T_\alpha(u)$ was proved in [2].

2.1.2. Stability of Solutions. Let u_α be the unique minimizer of T_α over \mathcal{C} given by Theorem 3. A similar analysis yields the existence and uniqueness of solutions $u_{\alpha,n}$ of (21) for $\alpha \geq 0$ provided that for each $n \in \mathbb{N}$, $A_n u \geq 0$ for all $u \in \mathcal{C}$ and $z_n \geq 0$. Problem (18), (19) is then said to be stable provided $A_n \rightarrow A$ and $z_n \rightarrow z + \gamma$ implies $u_{\alpha,n} \rightarrow u_\alpha$.

The following theorem (from [1]) gives conditions that guarantee this result. For completeness, we present the proof.

Theorem 4. *For each $n \in \mathbb{N}$, let $u_{\alpha,n}$ be the unique minimizer of $T_{\alpha,n}$ over \mathcal{C} , and suppose that*

(i) *for any sequence $\{u_n\} \subset L^p(\Omega)$,*

$$\lim_{n \rightarrow \infty} T_{\alpha,n}(u_n) = +\infty \quad \text{whenever} \quad \lim_{n \rightarrow \infty} \|u_n\|_{BV} = +\infty; \quad (31)$$

(ii) *given $M > 0$ and $\epsilon > 0$, there exists N such that*

$$|T_{\alpha,n}(u) - T_\alpha(u)| < \epsilon \quad \text{whenever} \quad n \geq N, \quad \|u\|_{BV} \leq M. \quad (32)$$

Then

$$\lim_{n \rightarrow \infty} \|u_{\alpha,n} - u_\alpha\|_p = 0 \quad (33)$$

for $1 \leq p < d/(d-1)$. If $d \geq 2$ and $p = d/(d-1)$ convergence is weak, i.e.

$$u_{\alpha,n} \rightharpoonup u_\alpha. \quad (34)$$

Proof. Note that $T_{\alpha,n}(u_{\alpha,n}) \leq T_{\alpha,n}(u_\alpha)$. From this and (32), we have

$$\limsup T_{\alpha,n}(u_{\alpha,n}) \leq T_\alpha(u_\alpha) < \infty. \quad (35)$$

Thus by (31), $\{u_{\alpha,n}\}$ is *BV*-bounded. By Theorem 1, there exists a subsequence $\{u_{\alpha,n_j}\}$ that converges (weakly) to some $\hat{u} \in L^p(\Omega)$. Furthermore, by the weak lower semicontinuity of T_α , (32), and (35) we have

$$\begin{aligned} T_\alpha(\hat{u}) &\leq \liminf T_\alpha(u_{\alpha,n_j}), \\ &= \liminf (T_\alpha(u_{\alpha,n_j}) - T_{\alpha,n_j}(u_{\alpha,n_j})) + \liminf T_{\alpha,n_j}(u_{\alpha,n_j}), \\ &\leq T_\alpha(u_\alpha). \end{aligned}$$

Since u_α is the unique minimizer of T_α , $\hat{u} = u_\alpha$. Since every convergent subsequence of $\{u_{\alpha,n}\}$ converges to u_α , we have that $u_{\alpha,n} \rightarrow u_\alpha$ (weakly if $p = d/(d-1)$). \square

The following corollary of Theorem 4 is the stability result for (18), (19) that we seek.

Corollary 1 (Stability of Minimizers). *Assume $1 \leq p < d/(d-1)$, $\|z_n - (z + \gamma)\|_\infty \rightarrow 0$, and that $A_n \rightarrow A$ in the $L^1(\Omega)$ operator norm. Then*

$$\lim_{n \rightarrow \infty} \|u_{\alpha,n} - u_\alpha\|_p = 0.$$

If $p = d/(d-1)$, then $u_{\alpha,n} \rightarrow u_\alpha$.

Proof. Without loss of generality, due to (22), we assume $\beta = 0$ and show that conditions (i) and (ii) from Theorem 4 hold. Also, all limits are assumed to be taken as $n \rightarrow \infty$.

For condition (i), we repeat the proof of Lemma 2. Taking $u_{\alpha,n} = v_{\alpha,n} + w_{\alpha,n}$, if $\|u_{\alpha,n}\|_{BV} \rightarrow \infty$, then either $J_0(v_{\alpha,n}) \rightarrow \infty$ or $\|w_{\alpha,n}\|_1 \rightarrow \infty$.

Since $T_{\alpha,n}(u_{\alpha,n}) \geq T_{0,n}(u_{0,n}) + \alpha J_0(v_{\alpha,n})$, we see that if $T_{0,n}(u_{0,n})$ is bounded below, $J_0(v_{\alpha,n}) \rightarrow \infty$ implies $T_\alpha(u_{\alpha,n}) \rightarrow \infty$. To see that $T_{0,n}(u_{0,n})$ is bounded below, we note that using the analogue of inequality (29) together with the properties of $x - c \log x$ for $c > 0$ yields $T_{0,n}(u) \geq \|z_n + \sigma^2\|_\infty - \|z_n + \sigma^2\|_\infty \log \|z_n + \sigma^2\|_\infty$, which has a lower bound for all n since $\|z_n - (z + \gamma)\|_\infty \rightarrow 0$ and $z \in L^\infty(\Omega)$.

On the other hand, if $\|u_{\alpha,n}\|_{BV} \rightarrow \infty$ and $J_0(v_{\alpha,n})$ is bounded, then $\|w_{\alpha,n}\|_1 \rightarrow \infty$, in which case from (30) we have

$$T_{\alpha,n}(u_{\alpha,n}) \geq C_2 \|w_{\alpha,n}\|_1 - M - \|z_n + \sigma^2\|_\infty \log(C_2 \|w_{\alpha,n}\|_1 + M), \quad (36)$$

where M is the upper bound on $\|A_n\|_1 C_1 J_0(v_{\alpha,n}) + (\gamma + \sigma^2)|\Omega|$ obtained using the uniform boundedness of both $\|A_n\|$ (Banach-Steinhaus) and $J_0(v_{\alpha,n})$. Since $\|z_n + \sigma^2\|_\infty$ is uniformly bounded, (36) implies $T_{\alpha,n}(u_{\alpha,n}) \rightarrow \infty$.

For condition (ii), note that, using Jensen's inequality and the properties of the logarithm,

$$\begin{aligned} |T_{\alpha,n}(u) - T_\alpha(u)| &= \left| \int_\Omega ((A_n - A)u - (z_n + \sigma^2) \log(A_n u + \gamma + \sigma^2)) \, dx \right. \\ &\quad \left. + \int_\Omega ((z + \gamma + \sigma^2) \log(Au + \gamma + \sigma^2)) \, dx \right|, \end{aligned}$$

$$\begin{aligned} &\leq \|A_n - A\|_1 \|u\|_1 + \|z_n - (z + \gamma)\|_\infty \log(\|A_n\|_1 \|u\|_1 + (\gamma + \sigma^2)|\Omega|) \\ &\quad + \|z + \gamma + \sigma^2\|_\infty \log\left\|\frac{(Au + \gamma + \sigma^2)}{(A_n u + \gamma + \sigma^2)}\right\|_1. \end{aligned} \quad (37)$$

By assumption, $\|A_n - A\|_1, \|z_n - (z + \gamma)\|_\infty \rightarrow 0$. Furthermore, by the Banach-Steinhaus Theorem, $\|A_n\|_1$ is uniformly bounded, and since we are assuming that $\|u\|_{BV}$ is bounded, by Theorem 1 we have that $\|u\|_1$ is bounded as well. Thus the first two terms on the right-hand side in (37) tend to zero as $n \rightarrow \infty$. For the third term note that

$$\left\|\frac{Au + \gamma + \sigma^2}{A_n u + \gamma + \sigma^2} - 1\right\|_1 \leq \left\|\frac{1}{A_n u + \gamma + \sigma^2}\right\|_1 \|A_n - A\|_1 \|u\|_1,$$

which converges to zero since $\|1/(A_n u + \gamma + \sigma^2)\|_1$ is bounded and $\|A_n - A\|_1 \rightarrow 0$. Thus $\log(\|(Au + \gamma + \sigma^2)/(A_n u + \gamma + \sigma^2)\|_1) \rightarrow \log(1) = 0$, and hence

$$|T_{\alpha,n}(u) - T_\alpha(u)| \rightarrow 0. \quad (38)$$

The desired result now follows from Theorem 4. \square

Finally, the main result of this subsection now follows directly from Theorem 3 and Corollary 1

Theorem 5 (Well-Posedness). *Problem (18), (19) is well-posed.*

2.2. Convergence of Minimizers

It remains to show that a sequence of positive regularization parameters $\{\alpha_n\}$ can be chosen so that $u_{\alpha_n,n} \rightarrow u_{\text{exact}}$ as $\alpha_n \rightarrow 0$.

Theorem 6 (Convergence of Minimizers). *Let $1 \leq p \leq d/(d-1)$. Suppose $\|z_n - (z + \gamma)\|_\infty \rightarrow 0$, $A_n \rightarrow A$ in the $L^1(\Omega)$ operator norm, and $\alpha_n \rightarrow 0$ at a rate such that*

$$(T_{0,n}(u_{\text{exact}}) - T_{0,n}(u_{0,n}))/\alpha_n \quad (39)$$

is bounded, where u_{exact} and $u_{0,n}$ are the unique minimizers of T_0 and $T_{0,n}$ respectively in \mathcal{C} . Then $u_{\alpha_n,n} \rightarrow u_{\text{exact}}$ strongly in $L^p(\Omega)$ for $1 \leq p < d/(d-1)$ and weakly for $p = d/(d-1)$.

Proof. Again, due to (22), it suffices to consider the $\beta = 0$ case. Since $u_{\alpha_n,n}$ minimizes $T_{\alpha_n,n}$, we have

$$T_{\alpha_n,n}(u_{\alpha_n,n}) \leq T_{\alpha_n,n}(u_{\text{exact}}). \quad (40)$$

Since $\{z_n\}$ and $\{A_n\}$ are uniformly bounded and $A_n \rightarrow A$ in the $L^1(\Omega)$ operator norm, $\{T_{\alpha_n,n}(u_{\text{exact}})\}$ is a bounded sequence, and (40) implies that $\{T_{\alpha_n,n}(u_{\alpha_n,n})\}$ is therefore also a bounded sequence.

Subtracting $T_{0,n}(u_{0,n})$ from each term in (40), dividing by α_n , and using the decomposition $u_{\alpha_n,n} = v_{\alpha_n,n} + w_{\alpha_n,n}$ yields

$$(T_{0,n}(u_{\alpha_n,n}) - T_{0,n}(u_{0,n}))/\alpha_n + J_0(v_{\alpha_n,n}) \leq (T_{0,n}(u_{\text{exact}}) - T_{0,n}(u_{0,n}))/\alpha_n + J_0(u_{\text{exact}}). \quad (41)$$

By (39), the right-hand side of (41) is bounded, implying the left hand side is bounded. Since $T_{0,n}(u_{\alpha_n,n}) - T_{0,n}(u_{0,n})$ is nonnegative, $J_0(v_{\alpha_n,n})$ is therefore also bounded. The boundedness of $T_{\alpha_n,n}(u_{\alpha_n,n})$ together with (36) imply that $\|u_{\alpha_n,n}\|_1$ is bounded. The BV -boundedness of $\{u_{\alpha_n,n}\}$ then follows from (27).

We show that $\|u_{\alpha_n,n} - u_{\text{exact}}\|_p \rightarrow 0$ ($u_{\alpha_n,n} \rightharpoonup u_{\text{exact}}$ for $p = d/(d-1)$) by showing that every subsequence of $\{u_{\alpha_n,n}\}$ contains a subsequence that converges to u_{exact} . Every subsequence $\{u_{\alpha_{n_j},n_j}\}$ of $\{u_{\alpha_n,n}\}$ is BV -bounded since $\{u_{\alpha_n,n}\}$ is, and by Theorem 1 has a convergent subsequence. Therefore, without loss of generality, we can assume that $\{u_{\alpha_{n_j},n_j}\}$ converges strongly (weakly for $p = d/(d-1)$) to some $\hat{u} \in L^p(\Omega)$. Then

$$\begin{aligned} T_0(\hat{u}) &= \int_{\Omega} (A(\hat{u} - u_{\alpha_{n_j},n_j}) + (A - A_{n_j})u_{\alpha_{n_j},n_j} + (z_{n_j} - (z + \gamma)) \log(A\hat{u} + \gamma + \sigma^2)) dx \\ &\quad - \int_{\Omega} (z_{n_j} + \sigma^2) \log((A_{n_j}u_{\alpha_{n_j},n_j} + \gamma + \sigma^2)/(A\hat{u} + \gamma + \sigma^2)) dx + T_{0,n_j}(u_{\alpha_{n_j},n_j}), \end{aligned}$$

which, as in previous arguments, yields

$$\begin{aligned} |T_{0,n_j}(u_{\alpha_{n_j},n_j}) - T_0(\hat{u})| &\leq \int_{\Omega} A(\hat{u} - u_{\alpha_{n_j},n_j}) dx \\ &\quad + \|z_{n_j} - (z + \gamma)\|_{\infty} \log(\|A\|_1 \|\hat{u}\|_1 + \gamma|\Omega|) \\ &\quad + \|z_{n_j} + \sigma^2\|_{\infty} \log\|(A_{n_j}u_{\alpha_{n_j},n_j} + \gamma + \sigma^2)/(A\hat{u} + \gamma + \sigma^2)\|_1 \\ &\quad + \|A - A_{n_j}\|_1 \|u_{\alpha_{n_j},n_j}\|_1. \end{aligned}$$

Then for $1 \leq p \leq d/d-1$,

$$\|z_{n_j} - (z + \gamma)\|_{\infty} \log(\|A\|_1 \|\hat{u}\|_1 + (\gamma + \sigma^2)|\Omega|) \rightarrow 0,$$

since $\|z_{n_j} - (z + \gamma)\|_{\infty} \rightarrow 0$ and $\log(\|A\|_1 \|\hat{u}\|_1 + (\gamma + \sigma^2)|\Omega|)$ is constant, and

$$\|A - A_{n_j}\|_1 \|u_{\alpha_{n_j},n_j}\|_1 \rightarrow 0$$

since $\|A - A_{n_j}\|_1 \rightarrow 0$ and $\|u_{\alpha_{n_j},n_j}\|_1$ is uniformly bounded.

Since A is a bounded linear operator and Ω is a set of finite measure, $F(u) = \int_{\Omega} Au dx$ is a bounded linear functional on $L^p(\Omega)$. The weak convergence of $\{u_{\alpha_{n_j},n_j}\}$ (recall that strong convergence implies weak convergence) then implies $\int_{\Omega} Au_{\alpha_{n_j},n_j} dx \rightarrow \int_{\Omega} A\hat{u} dx$, which yields $\int_{\Omega} A(\hat{u} - u_{\alpha_{n_j},n_j}) dx \rightarrow 0$.

Since A is compact, it is completely continuous, i.e. the weak convergence of $u_{\alpha_{n_j},n_j}$ to \hat{u} implies that $\|Au_{\alpha_{n_j},n_j} - A\hat{u}\|_1 \rightarrow 0$ (cf. [8, Prop. 3.3]). Thus, since $\left\| \frac{1}{A\hat{u} + \gamma + \sigma^2} \right\|_1$ is bounded, and

$$\begin{aligned} \left\| \frac{A_{n_j}u_{\alpha_{n_j},n_j} + \gamma + \sigma^2}{A\hat{u} + \gamma + \sigma^2} - 1 \right\|_1 &\leq \left\| \frac{1}{A\hat{u} + \gamma + \sigma^2} \right\|_1 \|A_{n_j}u_{\alpha_{n_j},n_j} - A\hat{u}\|_1, \\ &\leq \left\| \frac{1}{A\hat{u} + \gamma + \sigma^2} \right\|_1 \\ &\quad \times \left(\|A_{n_j} - A\|_1 \|u_{\alpha_{n_j},n_j}\|_1 + \|Au_{\alpha_{n_j},n_j} - A\hat{u}\|_1 \right), \end{aligned}$$

we have that $\|z_{n_j} + \sigma^2\|_\infty \log \|(A_{n_j} u_{\alpha_{n_j}, n_j} + \gamma + \sigma^2)/(A\hat{u} + \gamma + \sigma^2)\|_1 \rightarrow 0$. Therefore

$$T_0(\hat{u}) = \lim_{n_j \rightarrow \infty} T_{0, n_j}(u_{\alpha_{n_j}, n_j}).$$

Invoking (41), (39), and (38), respectively, yields

$$\lim_{n_j \rightarrow \infty} T_{0, n_j}(u_{\alpha_{n_j}, n_j}) = \lim_{n_j \rightarrow \infty} T_{0, n_j}(u_{0, n_j}) = \lim_{n_j \rightarrow \infty} T_{0, n_j}(u_{\text{exact}}) = T_0(u_{\text{exact}}).$$

Thus $T_0(\hat{u}) = T_0(u_{\text{exact}})$, and, since u_{exact} is the unique minimizer of T_0 , $\hat{u} = u_{\text{exact}}$. Therefore $\{u_{\alpha_{n_j}, n_j}\}$ converges strongly (weakly for $p = d/(d-1)$) to u_{exact} in $L^p(\Omega)$. \square

Remarks:

- We note that σ^2 can be taken to be zero in the likelihood functional (11) and the above results will still hold. Note that this is the case even if $\sigma^2 > 0$ in (5).
- In the denoising case, i.e. A identity, one need only prove existence and uniqueness of solutions. The analysis in Section 2.1.1 suffices for this result, however this was proved previously in [12].
- The above arguments can be modified to obtain the analogous results when standard Tikhonov regularization is used instead of total variation. This is the topic of [4], and the resulting computational problem is the topic of the work in [5, 3].

3. A Numerical Method

In this section, we present a numerical method and an experiment to demonstrate that total variation-penalized Poisson likelihood estimation can be effective in practice. For simplicity in presentation, we will use matrix-vector notation. In particular, by lexicographically ordering the $N \times N$ arrays $\{z_{ij}\}_{i,j=1}^N$, $\{u(\xi_r, \eta_s)\}_{r,s=1}^N$, and $\left\{\frac{1}{N^2} \sum_{r=1}^N \sum_{s=1}^N a_{ij}(\xi_r, \eta_s) u(\xi_r, \eta_s)\right\}$, we obtain the vectors \mathbf{z} , \mathbf{u} , and $\mathbf{A}\mathbf{u}$ respectively, where \mathbf{z} and \mathbf{u} are $N^2 \times 1$ and \mathbf{A} is $N^2 \times N^2$. Using this notation, the total variation regularized Poisson likelihood estimate will be the solution of the problem

$$\arg \min_{\mathbf{u} \geq \mathbf{0}} T_\alpha(\mathbf{u}) \stackrel{\text{def}}{=} T_0(\mathbf{u}) + \alpha J_\beta(\mathbf{u}), \quad (42)$$

where

$$T_0(\mathbf{u}) \stackrel{\text{def}}{=} \sum_{i=1}^{N^2} ([\mathbf{A}\mathbf{u}]_i + \gamma + \sigma^2) - \sum_{i=1}^{N^2} (z_i + \sigma^2) \log([\mathbf{A}\mathbf{u}]_i + \gamma + \sigma^2). \quad (43)$$

Here z_i is the i th component of \mathbf{z} , and $J_\beta(\mathbf{u})$ is the numerical approximation of (16) discussed below. In our experiments, β was taken to be 1.

The gradient and Hessian of $T_\alpha(\mathbf{u})$, as defined in (42), are given by

$$\begin{aligned} \nabla T_\alpha(\mathbf{u}) &= \nabla T_0(\mathbf{u}) + \alpha \nabla J_\beta(\mathbf{u}), \\ \nabla^2 T_\alpha(\mathbf{u}) &= \nabla^2 T_0(\mathbf{u}) + \alpha \nabla^2 J_\beta(\mathbf{u}). \end{aligned}$$

The gradient and Hessian of the Poisson likelihood functional $T_0(\mathbf{u})$ have expressions

$$\nabla T_0(\mathbf{u}) = \mathbf{A}^T \left(\frac{\mathbf{A}\mathbf{u} - (\mathbf{z} - \gamma)}{\mathbf{A}\mathbf{u} + \gamma + \sigma^2} \right), \quad (44)$$

$$\nabla^2 T_0(\mathbf{u}) = \mathbf{A}^T \left(\text{diag} \left(\frac{\mathbf{z} + \sigma^2}{(\mathbf{A}\mathbf{u} + \gamma + \sigma^2)^2} \right) \right) \mathbf{A}, \quad (45)$$

where $\text{diag}(\mathbf{v})$ is the diagonal matrix with \mathbf{v} as its main diagonal. Note the similarities with (12) and (13). Here, and in what follows, we will use \mathbf{x}/\mathbf{y} , where $\mathbf{x}, \mathbf{y} \in \mathbb{R}^{N^2}$, to denote Hadamard, or component-wise, division, and $\mathbf{x}^2 \stackrel{\text{def}}{=} \mathbf{x} \odot \mathbf{x}$, where “ \odot ” denotes the Hadamard product.

Note that for moderate to large values of σ^2 , say $\sigma^2 \geq 3^2$, it is extremely unlikely for the Gaussian $g(i) + \sigma^2$ from statistical model (6) to be negative. Then, since Poisson random variables take on only nonnegative integer values, the random variable $z_i + \sigma^2$ is also highly unlikely to be nonpositive. Furthermore, γ and σ^2 are both positive parameters and by assumption $\mathbf{A}\mathbf{u} \geq \mathbf{0}$ whenever $\mathbf{u} \geq \mathbf{0}$, where $\mathbf{v} \geq \mathbf{0}$ denotes component-wise nonnegativity for \mathbf{v} . Thus it can be reasonably assumed that $\nabla^2 T_\alpha(\mathbf{u})$ is positive definite for all $\mathbf{u} \geq \mathbf{0}$, in which case T_α has a unique minimizer over the set $\{\mathbf{u} \in \mathbb{R}^{N^2} \mid \mathbf{u} \geq \mathbf{0}\}$.

The gradient and Hessian of $J_\beta(\mathbf{u})$ require a bit more work. First, recall from (16) that in two-dimensions

$$J_\beta(u) = \int_\Omega \sqrt{\left(\frac{\partial u}{\partial x}\right)^2 + \left(\frac{\partial u}{\partial y}\right)^2 + \beta} dx dy, \quad (46)$$

which has discrete analogue

$$J_\beta(\mathbf{u}) = \Delta x \Delta y \sum_{i=1}^n \sum_{i=1}^n \sqrt{(\mathbf{D}_x \mathbf{u})^2 + (\mathbf{D}_y \mathbf{u})^2 + \beta}, \quad (47)$$

where \mathbf{D}_x and \mathbf{D}_y are $N^2 \times N^2$ matrices corresponding to the grid approximations of the first derivative with respect to x and y respectively. For our implementation, the average of the two regularization terms resulting from the use of first-order upwind differencing and first-order downwind differencing for \mathbf{D}_x and \mathbf{D}_y was used. Thus the resulting approximation will also be first-order accurate. Midpoint quadrature is used to discretize the integral in (46).

We now provide the formulas for the gradient and Hessian of J_β , and, in order to simplify notation, we drop the $\Delta x \Delta y$ term in (47). The gradient and Hessian of J_β are given by

$$\begin{aligned} \nabla J_\beta(\mathbf{u}) &= \mathbf{L}_1(\mathbf{u})\mathbf{u}, \\ \nabla^2 J_\beta(\mathbf{u}) &= \mathbf{L}_1(\mathbf{u}) + 2\mathbf{L}_2(\mathbf{u}), \end{aligned} \quad (48)$$

where, if $\psi(t) \stackrel{\text{def}}{=} \sqrt{t + \beta}$, $D\mathbf{u}^2 \stackrel{\text{def}}{=} (\mathbf{D}_x \mathbf{u})^2 + (\mathbf{D}_y \mathbf{u})^2$, and $\mathbf{D}_x \mathbf{u} \mathbf{D}_y \mathbf{u} \stackrel{\text{def}}{=} \mathbf{D}_x \mathbf{u} \odot \mathbf{D}_y \mathbf{u}$,

$$\mathbf{L}_1(\mathbf{u}) = [\mathbf{D}_x^T \mathbf{D}_y^T] \begin{bmatrix} \text{diag}(\psi'(D\mathbf{u}^2)) & \mathbf{0} \\ \mathbf{0} & \text{diag}(\psi'(D\mathbf{u}^2)) \end{bmatrix} \begin{bmatrix} \mathbf{D}_x \\ \mathbf{D}_y \end{bmatrix}, \quad (49)$$

$$\mathbf{L}_2(\mathbf{u}) = [\mathbf{D}_x^T \mathbf{D}_y^T] \begin{bmatrix} \text{diag}((\mathbf{D}_x \mathbf{u})^2 \odot \psi''(D\mathbf{u}^2)) & \text{diag}(\mathbf{D}_x \mathbf{u} \mathbf{D}_y \mathbf{u} \odot \psi''(D\mathbf{u}^2)) \\ \text{diag}(\mathbf{D}_x \mathbf{u} \mathbf{D}_y \mathbf{u} \odot \psi''(D\mathbf{u}^2)) & \text{diag}((\mathbf{D}_y \mathbf{u})^2 \odot \psi''(D\mathbf{u}^2)) \end{bmatrix} \begin{bmatrix} \mathbf{D}_x \\ \mathbf{D}_y \end{bmatrix}.$$

For a more detailed treatment of these computations see [22, Chapter 8].

3.1. The Projected Lagged-Diffusivity Method

The *active set* for $\mathbf{u} \geq \mathbf{0}$ is defined

$$\mathcal{A}(\mathbf{u}) = \{i \mid u_i = 0\}.$$

The complementary set of indices is called the *inactive set* and is denoted by $\mathcal{I}(\mathbf{u})$. The orthogonal projection of a vector $\mathbf{u} \in \mathbb{R}^{N^2}$ onto $\{\mathbf{x} \in \mathbb{R}^{N^2} \mid \mathbf{x} \geq \mathbf{0}\}$ is given by

$$\mathcal{P}(\mathbf{u}) = \max\{\mathbf{u}, \mathbf{0}\},$$

where the maximum is computed component-wise. Finally, let $\mathbf{D}_{\mathcal{I}}(\mathbf{u})$ denote the diagonal matrix with components

$$[\mathbf{D}_{\mathcal{I}}(\mathbf{u})]_{ii} = \begin{cases} 1, & i \in \mathcal{I}(\mathbf{u}) \\ 0, & i \in \mathcal{A}(\mathbf{u}). \end{cases} \quad (50)$$

Then $\mathbf{D}_{\mathcal{A}}(\mathbf{u}) \stackrel{\text{def}}{=} \mathbf{I} - \mathbf{D}_{\mathcal{I}}(\mathbf{u})$, where \mathbf{I} is the $N^2 \times N^2$ identity matrix.

We now present our computational method for solving (42). The most straightforward computational method for use on nonnegatively constrained problems is the projected gradient algorithm [11]. However, for this problem, projected gradient is slow to converge. We therefore advocate using *projected lagged-diffusivity*. A general formulation of the method is as follows: given \mathbf{u}_k , compute

$$\mathbf{H}_k = \mathbf{D}_{\mathcal{I}}^k \nabla^2 T_0(\mathbf{u}_k) \mathbf{D}_{\mathcal{I}}^k + \alpha \mathbf{D}_{\mathcal{I}}^k \mathbf{L}_1(\mathbf{u}_k) \mathbf{D}_{\mathcal{I}}^k + \mathbf{D}_{\mathcal{A}}^k, \quad (51)$$

$$\mathbf{v}_k = -\mathbf{H}_k^{-1} \nabla T_{\alpha}(\mathbf{u}_k) = -\mathbf{H}_k^{-1} (\mathbf{D}_{\mathcal{I}}^k \nabla T_{\alpha}(\mathbf{u}_k)) - \mathbf{D}_{\mathcal{A}}^k \nabla T_{\alpha}(\mathbf{u}_k); \quad (52)$$

$$\lambda_k = \arg \min_{\lambda > 0} T_{\alpha}(\mathcal{P}(\mathbf{u}_k + \lambda \mathbf{v}_k)); \quad (53)$$

$$\mathbf{u}_{k+1} = \mathcal{P}(\mathbf{u}_k + \lambda_k \mathbf{v}_k). \quad (54)$$

Here $\mathbf{D}_{\mathcal{A}}^k \stackrel{\text{def}}{=} \mathbf{D}_{\mathcal{A}}(\mathbf{u}_k)$ and $\mathbf{D}_{\mathcal{I}}^k \stackrel{\text{def}}{=} \mathbf{D}_{\mathcal{I}}(\mathbf{u}_k)$.

The method is called projected lagged-diffusivity because, if

$$T_0(\mathbf{u}) = \frac{1}{2} \|\mathbf{A}\mathbf{u} - \mathbf{z}\|_2^2, \quad (55)$$

the nonnegativity constraints are dropped so that $\mathbf{D}_{\mathcal{I}}^k = \mathbf{I}$ and $\mathbf{D}_{\mathcal{A}}^k = \mathbf{0}$ for all k , and $\lambda_k = 1$ for all k , the lagged-diffusivity fixed-point iteration results (c.f. [22]).

For large-scale problems, such as the one that we consider, the projected quasi-Newton step (51), (52) can only be computed approximately. Since $\nabla^2 T_{\alpha}(\mathbf{u}_k)$ is symmetric, positive-definite, so is \mathbf{H}_k . Thus, conjugate gradient (CG) iterations can be used for solving $\mathbf{H}_k \mathbf{v} = -\mathbf{D}_{\mathcal{I}}^k \nabla T_{\alpha}(\mathbf{u}_k)$. It can be shown that CG will compute the exact solution in a finite number of iterations, but this is not practical for large-scale problems. The remedy is to truncate CG iterations using a stopping criterion that will

not effect the theoretical convergence properties of the method. In our implementation of CG, we use initial guess $\mathbf{v}_k^0 = \mathbf{0}$ with stopping criterion

$$\|\mathbf{H}_k \mathbf{v}_k^j + \mathbf{D}_{\mathcal{I}}^k \nabla T_\alpha(\mathbf{u}_k)\| \leq \min \left\{ \frac{1}{2}, \|\mathbf{D}_{\mathcal{I}}^k \nabla T_\alpha(\mathbf{u}_k)\| \right\} \cdot \|\mathbf{D}_{\mathcal{I}}^k \nabla T_\alpha(\mathbf{u}_k)\|, \quad (56)$$

where \mathbf{v}_k^j is the j th CG iterate at outer iteration k . CG stopping criteria of this type are standard [14]. In addition, we use the stopping criteria

$$j = \text{CG}_{\max}. \quad (57)$$

That is, if either (56) or (57) hold, CG iterations are stopped and \mathbf{v}_k in (52) is taken to be the most recent CG iterate. Then \mathbf{v}_k can be guaranteed to be a descent direction, making it appropriate for use in the line search subproblem (53).

We note that in the numerical example below, the use of (57) is necessary in order to prevent an excessive number of CG iterations per outer iteration. This suggests the use of a CG stopping criterion that is more robust than (56) to increase computational efficiency, a possibility to be explored in future work.

Because T_α is not a quadratic function, the line search subproblem (53) must also be approximately solved. A standard approach is to do this iteratively using a backtracking line search algorithm. In our implementation, we use the quadratic backtracking line search scheme of [13], which generates a finite decreasing sequence of approximate solutions $\{\lambda_k^r\}_{r=1}^m$, where m is the smallest integer such that the sufficient decrease condition

$$T_\alpha(\mathcal{P}(\mathbf{u}_k + \lambda_k^r \mathbf{v}_k)) \leq T_\alpha(\mathbf{u}_k) + \mu \langle \nabla T_\alpha(\mathbf{u}_k), \mathcal{P}(\mathbf{u}_k + \lambda_k^r \mathbf{v}_k) - \mathbf{u}_k \rangle$$

holds. In our implementation, $\mu = 0.1$, which is what is used in [13].

Finally, we stop projected Newton iterations based on the value of the norm of the projected gradient, which is defined by

$$\nabla_{\text{proj}} T_\alpha(\mathbf{u}_k) \stackrel{\text{def}}{=} \mathbf{D}_{\mathcal{I}}^k \nabla T_\alpha(\mathbf{u}_k) + \min\{\mathbf{0}, \mathbf{D}_{\mathcal{A}}^k \nabla T_\alpha(\mathbf{u}_k)\},$$

noting that since T_α is strictly convex, \mathbf{u}^* solves (42) if and only if $\nabla_{\text{proj}} T_\alpha(\mathbf{u}^*) = \mathbf{0}$. This motivates the following stopping criteria for the outer iterations:

$$\|\nabla_{\text{proj}} T_\alpha(\mathbf{u}_k)\| / \|\nabla_{\text{proj}} T_\alpha(\mathbf{u}_0)\| < \text{GradTol}, \quad (58)$$

where GradTol is a small positive number.

Remarks:

- The projected Newton method [7, 11] results if (51) is replaced by the reduced Hessian

$$\mathbf{H}_k = \mathbf{D}_{\mathcal{I}}^k \nabla^2 T_\alpha(\mathbf{u}_k) \mathbf{D}_{\mathcal{I}}^k + \mathbf{D}_{\mathcal{A}}^k, \quad (59)$$

but the resulting method is less computationally efficient.

- One possibility for improving the performance of our method is to precondition the CG iterations. Preconditioning is made difficult in this case because the form of \mathbf{H}_k changes nontrivially as the active set changes. Nonetheless, effective techniques have been introduced within similar contexts (c.f. [5, 3]).

Other methods have been introduced for edge preserving, Poisson likelihood estimation. For example, in [21], a regularization functional is introduced that incorporates information about the location of the edges within the image. The scheme has two stages: (i) solve a PDE-based edge detection problem for the current iterate \mathbf{u}_k ; then (ii) compute a new iterate \mathbf{u}_{k+1} by solving a regularized Poisson likelihood estimation problem, where the regularization term uses the edge map computed in stage (i). These steps are alternated until a stable reconstruction is obtained. This method has the benefit that the penalty term used in stage (ii) for regularization is quadratic, which is not the case for total variation regularization. Also, for images with smooth edges, the above scheme may be superior, since it is often the case that total variation regularization will give piecewise constant reconstructions even when they are not desirable. However interspersing a large-scale optimization problem with a large-scale PDE-based edge detection problem is computationally intensive. One clear benefit of using the approach presented here is that no alternating scheme is needed, which is likely to make computations more efficient.

Regularized Poisson likelihood estimation has also been approached from the Bayesian point of view. In particular, in [2, 16, 17] maximum a posteriori (MAP) denoising of images with Poisson noise statistics is studied. In [10], the MAP formulation of standard least squares total variation denoising is given. These ideas are then extended to the Poisson denoising problem in [2], where a simple gradient descent algorithm is given for computing the MAP estimate. The key concept for the MAP formulation of total variation denoising is the connection between total-variation regularization and the Laplace distribution [10], which, incidentally, can be used to formulate (42) as a MAP estimation problem as well. This connection is also exploited in [17]. In [16], a wavelet basis is used, and the Poisson likelihood with an ℓ_1 penalty on the wavelet coefficients is minimized. We note that our computational method is applicable to the Poisson denoising problem (set $\mathbf{A} = \mathbf{I}$ in (42)), which is the problem of focus for the above methods. This method, however, has been introduced in the more general context of image deblurring. Since deblurring optimization problems tend to be more challenging than the corresponding denoising problems, the effectiveness of the above methods for deblurring is not immediately apparent. In [15], however, a medical imaging deblurring problem is considered. Here a MAP estimate is computed using the EM algorithm. A conjugate prior approach is taken in order to make the approach computationally feasible. The resulting prior consists of a combination of gamma and beta densities.

In [5], an efficient computational method is introduced for solving (42) with $J_\beta(\mathbf{u})$ replaced by $\|\mathbf{u}\|_2^2$, i.e. standard Tikhonov regularization. Perhaps the most commonly used method for Poisson likelihood estimation is Richardson-Lucy (RL) iteration [6, 22]. When RL is used, regularization is implemented via the early truncation of iterations. In the next subsection, we compare the results obtain from these two approaches with those obtained using the approach presented here.

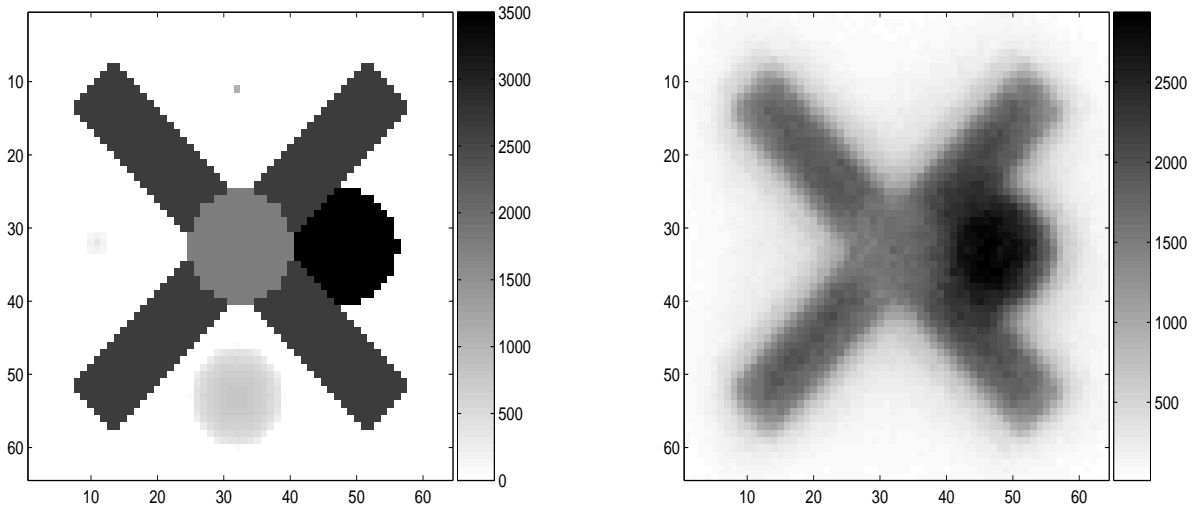


Figure 1. *Object and Blurred, Noisy Image.* On the left is the true object \mathbf{u}_{true} . On the right, is the blurred, noisy image \mathbf{z} .

3.2. A Numerical Experiment

In this subsection we present a numerical experiment to show that total variation-regularized Poisson likelihood estimation can be effective in practice and that results obtained with this approach compare well with those obtained using other methods.

In our experiment, the 64×64 true object $\mathbf{u}_{\text{exact}}$ is given on the left-hand side in Figure 1. Note that while the satellite is piecewise constant, the object also contains three two-dimensional Gaussians and one half-sphere; these sub-objects will be more visible when we present the comparisons below. A spatially invariant PSF is used to define the $64^2 \times 64^2$ blurring matrix \mathbf{A} . We follow the Fourier optics PSF model [22, Section 5.1.1], and hence, \mathbf{A} is a block Toeplitz with Toeplitz blocks (BTTB) matrix. For efficient computations, \mathbf{A} is embedded in a $128^2 \times 128^2$ block circulant with circulant block (BCCB) matrix, which can be diagonalized by the two-dimensional discrete Fourier and inverse discrete Fourier transform matrices [22]. Thus though results are shown on a 64×64 computational grid, computations are done on a 128×128 computational grid. Data \mathbf{z} with a signal-to-noise ratio of 30 is then generated using statistical model (7) with $\sigma^2 = 25$ and $\gamma = 10$ – physically realistic values for these parameters. To generate Poisson noise, the `poissrnd` function in MATLAB’s Statistics Toolbox is used. The corresponding blurred, noisy data \mathbf{z} is given on the right hand side in Figure 1.

With the blurred, noisy data in hand, we estimate $\mathbf{u}_{\text{exact}}$ by solving (42) using the projected lagged-diffusivity method with $\text{CG}_{\text{max}} = 50$ and $\text{GradTol} = 10^{-5}$. We chose these values for CG_{max} and GradTol in order to balance computational efficiency with good convergence properties of the method. Our initial guess was $\mathbf{u}_0 = \mathbf{1}$, and the regularization parameter was taken to be $\alpha = 5 \times 10^{-5}$. This choice of parameter

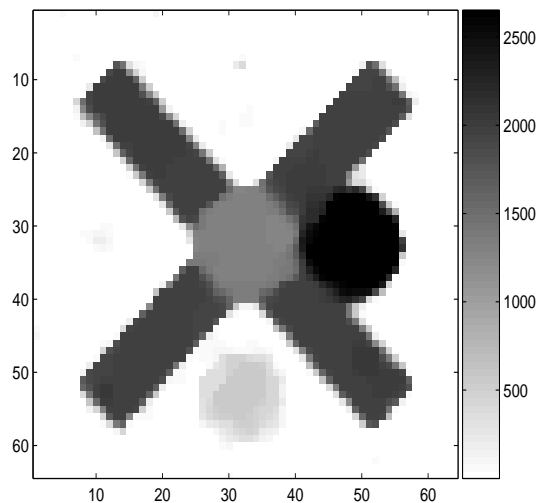


Figure 2. *Reconstruction of the object obtained using the projected lagged-diffusivity method.*

approximately minimizes $\|\mathbf{u}_\alpha - \mathbf{u}_{\text{exact}}\|$. The reconstruction is given in Figure 2.

In order to compare this result with those obtained using other methods, we will compare plots of cross sections of reconstructions corresponding to the 32nd row and 32nd column; note that the sub-objects are all centered on one of these two cross-sections. In our first comparison, we plot reconstructions obtained using our approach, RL, and the projected Newton method applied to the problem of minimizing the Tikhonov regularized Poisson likelihood function over $\{\mathbf{u} \mid \mathbf{u} \geq \mathbf{0}\}$. For the latter method, we use $\text{CG}_{\text{max}} = 50$, $\text{GradTol} = 10^{-8}$, and initial guess $\mathbf{u}_0 = \mathbf{1}$. The regularization parameter - chosen as above - was $\alpha = 2 \times 10^{-6}$. The RL reconstruction was taken to be the iterate that minimizes $\|\mathbf{u}_k - \mathbf{u}_{\text{exact}}\|$. The results are given in Figure 3. The total variation reconstruction is visually superior to the others, with the exception of the Gaussian with the high peak in the left-hand plot. This is not surprising given the fact that it has been observed that standard Poisson estimation is particularly effective at reconstructing objects with high intensity, but small support, such as a star.

The dominant cost in implementing each of the above algorithms is the computation of fast Fourier and inverse fast Fourier transforms (FFTs). For RL the total number of FFTs was 722. When projected Newton iteration was used on the Tikhonov regularized Poisson likelihood, 668 FFTs were needed before the stopping criteria were met. Finally, 25876 FFTs were needed in order to meet the stopping criteria for the total variation reconstruction. However, given the fact that (57) was met at 125 out of 135 outer iterations, it is our belief that with a more robust stopping criterion, the computational cost could be reduced substantially. Also, excellent results are obtained by projected lagged-diffusivity with a stopping criteria of $\text{GradTol} = 10^{-4}$ (see the comparisons

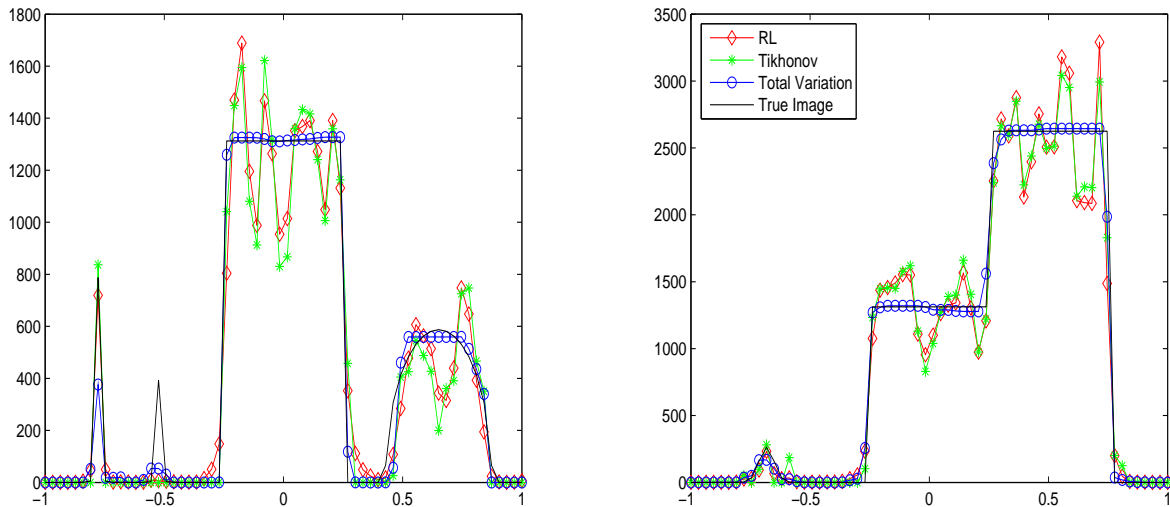


Figure 3. Comparison of Cross-Sections of Reconstructions Obtained with a Variety of Poisson Likelihood Methods. The left-hand plot corresponds to column 32 and the right-hand plot corresponds to row 32 of the respective reconstructions. The true image is the solid line; the projected lagged-diffusivity reconstruction is the line with circles; the Tikhonov solution is the line with stars; and the Richardson-Lucy solution is the line with diamonds.

below), and the total number of FFTs needed in this case is less by more than a factor of 4. Nonetheless, total variation estimation is clearly the most expensive of these three methods.

Finally, we compare the results obtained using our approach with those obtained using total variation regularization with a least squares likelihood. As was mentioned above, the projected lagged-diffusivity method can just as easily be used with T_0 given by (55). Thus we compare the results with these two different likelihood functions. We also implement standard lagged-diffusivity fixed point iteration. As one might expect, better results are obtained when the Poisson likelihood is used. This can be seen by the cross-section plots in Figure 4, although a comparison between the reconstruction given in Figures 2 and 5 shows that large scale features are reconstructed similarly whether the Poisson likelihood with nonnegativity constraint or the least squares likelihood without constraints is used. Note in particular the reconstructions of the sub-objects with narrow support. However, somewhat surprisingly, using the Poisson likelihood also greatly improves the computational efficiency of the method. In particular, with $\text{GradTol} = 10^{-4}$ and $\text{CG}_{\max} = 50$, lagged-diffusivity with $\alpha = 5 \times 10^{-2}$ required 45404 FFTs to meet GradTol , projected lagged-diffusivity with (55) and $\alpha = 5 \times 10^{-2}$ required 25074 FFTs and projected lagged-diffusivity with (43) and $\alpha = 5 \times 10^{-5}$ required 3628 FFTs. A possible explanation of this is that when projected lagged-diffusivity with (55) is used, the size of the active set at the resulting solution is only 19. Thus the nonnegativity constraints have little, if any, effect. Whereas for projected lagged-

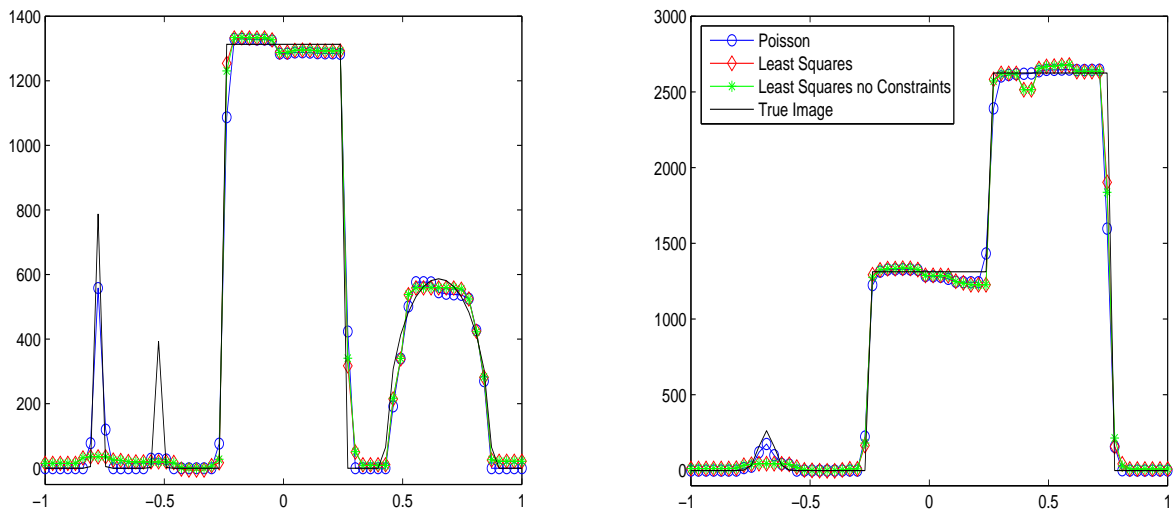


Figure 4. Comparison of Cross-Sections of Reconstructions Obtained with a Variety of Total Variation Methods. The left-hand plot corresponds to column 32 and the right-hand plot corresponds to row 32 of the respective reconstructions. The true image is the solid line; the projected lagged-diffusivity reconstruction with Poisson likelihood is the line with circles; the projected lagged-diffusivity reconstruction with least squares likelihood is the line with diamonds; the lagged-diffusivity reconstruction is the line with stars.

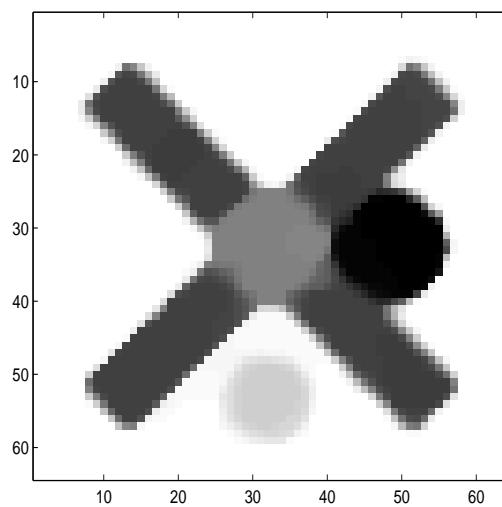


Figure 5. Reconstruction of the object obtained using the projected lagged-diffusivity method.

diffusivity with (43), the size of the active set at the resulting solution is 1511, or greater than 1/3 of the total number of pixels. This has the effect of reducing the size of the linear system that CG has to approximately solve by the same amount. The reason for why the active set is larger when (43) is used is unknown to us. In any event, our results suggest that one should consider using the Poisson likelihood together with a nonnegativity constraint when using total variation on large-scale problems.

4. Conclusions

In image deblurring problems, the collected data is a realization of a random vector whose components are, in many cases, accurately modeled by a Poisson distribution. The least squares approach is commonly used nonetheless, due in large part to the facts that the resulting methods are straightforward to implement and that regularization in conjunction with least squares data fitting has been extensively studied and stands on firm theoretical footings. It is our belief that similar theoretical foundations should be developed for regularization approaches in which the fit-to-data functional is not of least squares type. In this paper, we have considered the Poisson likelihood fit-to-data functional in conjunction with total variation regularization. The *a priori* knowledge of the nonnegativity of the true image is incorporated into the corresponding variational (constrained minimization) problem (18), (19). In our theoretical arguments, we first proved that (18), (19) is a well-posed problem for all $\alpha > 0$. We then showed that given a sequence of perturbed problems $z_n = A_n u$ such that $z_n \rightarrow z$ and $A_n \rightarrow A$, a sequence of nonnegative regularization parameters $\{\alpha_n\}$ can be chosen so that the corresponding minimizers $u_{\alpha_n, n}$ of (21) converge to the exact solution u_{exact} of (1) as $\alpha_n \rightarrow 0$.

We also verified the practical validity of total variation-penalized Poisson likelihood estimation by implementing the approach numerically. This required that we numerically solve the nonnegatively constrained minimization problem (42). For this, we introduced the projected lagged-diffusivity method. Our numerical results suggest that this method is quite effective in practice, as it compared favorably with Tikhonov regularized Poisson likelihood estimation, Richardson-Lucy, and least squares total variation. Perhaps most surprisingly, we found that using the Poisson likelihood together with nonnegativity constraints yields a more computationally efficient method than does the use of the least squares likelihood, with or without nonnegativity constraints, for total variation deblurring. This suggests that for large-scale total variation deblurring problems, one ought to consider using the Poisson likelihood with nonnegativity constraints in place of the least squares likelihood.

5. Acknowledgements

This work was supported by the NSF under grant DMS-0504325, by the University of Montana through its International Exchange Program, and by the University of Helsinki, which hosted the author during the 2006-07 academic year.

6. References

- [1] R. Acar and C.R. Vogel, *Analysis of bounded variation penalty methods for ill-posed problems*, Inverse Problems, 10 (1994), pp. 1217-1229.
- [2] T. Asaki, R. Chartrand and T. Le, *A Variational Approach to Reconstructing Images Corrupted by Poisson Noise*, UCLA CAM Report 05-49, November 2005.
- [3] Johnathan M. Bardsley, *A Limited Memory, Quasi-Newton Preconditioner for Nonnegatively Constrained Image Reconstruction*, Journal of the Optical Society of America A, vol. 21, no. 5, 2004, pp. 724-731.
- [4] J. M. Bardsley and N'djekornom Laobeul, *Tikhonov Regularization for Ill-Posed Poisson Likelihood Estimation: Analysis and Computation*, Inverse Problems in Science and Engineering, to appear.
- [5] J. M. Bardsley and C. R. Vogel, *A Nonnegatively Constrained Convex Programming Method for Image Reconstruction*, SIAM Journal on Scientific Computing, 25(4), 2004, pp. 1326-1343.
- [6] M. Bertero and P. Boccacci, *Introduction to Inverse Problems in Imaging*, Institute of Physics Publishing, 1998.
- [7] D. P. Bertsekas, *Projected Newton Methods for Optimization Problems with Simple Constraints*, SIAM Journal on Control and Optimization, **20** (1982), pp. 221-246.
- [8] John B. Conway, *A Course in Functional Analysis*, Second Edition, Springer, 1990.
- [9] W. Feller, *An Introduction to Probability Theory and Its Applications*, Wiley, New York, 1971.
- [10] M. Green, *Statistics of images, the TV algorithm of Rudin-Osher-Fatemi for image denoising, and an improved denoising algorithm*, CAM Report 02-55, UCLA, October 2002.
- [11] C. T. Kelley, *Iterative Methods for Optimization*, SIAM, Philadelphia, 1999.
- [12] T. Le, R. Chartrand, and T. J. Asaki, *A Variational Approach to Reconstructing Images Corrupted by Poisson Noise*, Journal of Mathematical Imaging and Vision, vol. 27, Issue 3, pp. 257-263.
- [13] J. J. Moré and G. Toraldo, *On the Solution of Large Quadratic Programming Problems with Bound Constraints*, SIAM Journal on Optimization, **1** (1991), pp. 93-113.
- [14] J. Nocedal and S. Wright, *Numerical Optimization*, Springer 1999.
- [15] Robert Nowak and Eric Kolaczyk, *A Statistical Multiscale Framework for Poisson Inverse Problems*, IEEE Transactions on Information Theory, 46(5), 2000, pp. 1811-1825.
- [16] Sylvain Sardy, Anestis Antoniadis, and Paul Tseng, *Automatic Smoothing with Wavelets for a Wide Class of Distributions*, Journal of Computational and Graphical Statistics, 13(2), 2004, pp.1-23.
- [17] Sylvain Sardy and Paul Tseng, *On the statistical analysis of smoothing by maximizing dirty Markov random field posterior distributions*, Journal of the American Statistical Association, Vol. 99(465), 2004, pp. 191-204(14).
- [18] D. L. Snyder, A. M. Hammoud, and R. L. White, *Image recovery from data acquired with a charge-coupled-device camera*, Journal of the Optical Society of America A, **10** (1993), pp. 1014-1023.
- [19] D. L. Snyder, C. W. Helstrom, A. D. Lanterman, M. Faisal, and R. L. White, *Compensation for readout noise in CCD images*, Journal of the Optical Society of America A, **12** (1995), pp. 272-283.
- [20] A. N. Tikhonov, A. V. Goncharsky, V. V. Stepanov and A. G. Yagola, *Numerical Methods for the Solution of Ill-Posed Problems*, Kluwer Academic Publishers, 1990.
- [21] Daniel F. Yu and Jeffrey A. Fessler, *Edge-Preserving Tomographic Reconstruction with Nonlocal Regularization*, IEEE Trans. on Medical Imaging, 21(2), 2002, pp. 159-173.
- [22] C. R. Vogel, *Computational Methods for Inverse Problems*, SIAM, Philadelphia, 2002.
- [23] C. R. Vogel and M. E. Oman, *A fast, robust algorithm for total variation based reconstruction of noisy, blurred images*, IEEE Transactions on Image Processing, **7** (1998), pp. 813-824.
- [24] E. Zeidler, *Applied Functional Analysis: Main Principles and their Applications*, Springer-Verlag, New York, 1995.